Taylor & Francis
Taylor & Francis Group

RESEARCH PAPER

🔓 OPEN ACCESS   🔄 Check for updates

Autophagy critically controls skin inflammation and apoptosis-induced stem cell activation

Lisette Van Hove[a,b,c], Annagiada Toniolo[a,b,c], Mohammad Ghiasloo[a,b,d], Kim Lecomte[a,b,c], Fleur Boone[a,b,c], Maarten Ciers[a,b,c], Kris Raaijmakers[a,b,c], Niels Vandamme[a,e], Jana Roels[a,e], Sophia Maschalidi[a,b], Kodi S Ravichandran[a,b], Maria Kasper[f], Geert van Loo[a,b,c], and Esther Hoste[a,b,c]

aVIB Center for Inflammation Research, Ghent, Belgium; bDepartment of Biomedical Molecular Biology, Ghent University, Ghent, Belgium; cCancer Research Institute Ghent (CRIG), Ghent, Belgium; dDepartment of Plastic and Reconstructive Surgery, Ghent University Hospital, Ghent, Belgium; eVIB Single Cell Core, Ghent-Leuven, Belgium; fDepartment of Cell and Molecular Biology, Karolinska Institutet, Stockholm, Sweden

ABSTRACT

Macroautophagy/autophagy is a cellular recycling program regulating cell survival and controlling inflammatory responses in a context-dependent manner. Here, we demonstrate that keratinocyte-selective ablation of *Atg16l1*, an essential autophagy mediator, results in exacerbated inflammatory and neoplastic skin responses. In addition, mice lacking keratinocyte autophagy exhibit precocious onset of hair follicle growth, indicating altered activation kinetics of hair follicle stem cells (HFSCs). These HFSCs also exhibit expanded potencies in an autophagy-deficient context as shown by *de novo* hair follicle formation and improved healing of abrasion wounds. ATG16L1-deficient keratinocytes are markedly sensitized to apoptosis. Compound deletion of RIPK3-dependent necroptotic and CASP8-dependent apoptotic responses or of TNFRSF1A/TNFR1 reveals that the enhanced sensitivity of autophagy-deficient keratinocytes to TNF-dependent cell death is driving altered activation of HFSCs. Together, our data demonstrate that keratinocyte autophagy dampens skin inflammation and tumorigenesis but curtails HFSC activation by restraining apoptotic responses.

Abbreviations: ATG16L1: autophagy related 16 like 1; DMBA: 2,4-dimethoxybenzaldehyde; DP: dermal papilla; EpdSCs: epidermal stem cells; Gas6: growth arrest specific 6; HF: hair follicle; HFSC: hair follicle stem cell; IFE: interfollicular epidermis; KRT5: keratin 5; MAP1LC3/LC3: microtubule-associated protein 1 light chain 3; PMK: primary mouse keratinocyte; RIPK3: receptor-interacting serine-threonine kinase 3; scRNAseq: single-cell RNA-sequencing; SG: sebaceous gland; TEWL: transepidermal water loss; TPA: 12-O-tetradecanoylphorbol-13-acetate; TNF: tumor necrosis factor; TNFRSF1A/TNFR1: tumor necrosis factor receptor superfamily, member 1a; UMAP: uniform manifold approximation and projection

Introduction

The skin provides a crucial barrier that protects our body from dehydration, environmental insults and occasional wounding. This epidermal barrier is maintained by continuous proliferation of keratinocyte stem cells (SCs) present in the basal layer of the interfollicular epidermis, termed epidermal SCs (EpdSCs). These EpdSCs generate keratinocytes that can undergo a tightly orchestrated differentiation program, resulting in the formation of the *stratum corneum* constituted by terminally differentiated corneocytes [1]. A second population of keratinocyte SCs, namely hair follicle SCs (HFSCs), resides in a distinct niche in the lower part of the hair follicle (HF) referred to as the bulge. HFs are cycling mini-organs that undergo periods of growth (anagen), followed by degeneration marked by extensive cell death (catagen) and a subsequent resting phase (telogen). Catagen, the regression stage of the hair cycle, is a unique example of an orchestrated, immunologically-silent death of keratinocytes, which in mice

is precisely timed and synchronized in the first two postnatal hair cycles [2]. The function of HFSCs is to maintain the HF during hair cycling and HF growth, a process that is mediated by reciprocal signaling between HFSCs and a specialized population of dermal fibroblasts located at the bottom of the hair, named the dermal papilla (DP) [3]. Upon wounding of the skin or during tumor formation, HFSCs can migrate from their homeostatic niche to the interfollicular epidermis (IFE) where they show remarkable plasticity and exhibit functions beyond their normal repertoire [4–6].

Polymorphisms in the human autophagy-related gene *ATG16L1* have been linked to immunological skin disorders, such as psoriasis vulgaris [7] and palmoplantar pustulosis [8], indicating an important role for autophagy in skin immunosurveillance. Macroautophagy (from here on referred to as autophagy) is a cellular process enabling degradation and recycling of proteins and organelles. The cytoplasmatic material that will be recycled is sequestered into a double-membrane vesicle, the

---

autophagosome, that completes degradation through fusion with a lysosome. Expansion and completion of the autophagosome relies on two ubiquitin-like conjugation systems: ATG7 (autophagy related 7) and ATG10 facilitate the covalent conjugation of ATG12 and ATG5, followed by binding to ATG16L1 (autophagy related 16 like 1). This multiprotein complex facilitates the conjugation of MAP1LC3/LC3 (microtubule-associated protein 1 light chain 3)-I to the phagophore membrane, a critical step to complete autophagy [9]. Next to its role in cellular recycling, the autophagic pathway also controls immune processes as it selectively degrades intracellular pathogens, damaged organelles and protein aggregates [10].

Here, we investigated the role of autophagy in skin conditions marked by elevated keratinocyte stem cell activation, namely inflammation, regeneration, tumorigenesis and hair cycling. For this, we studied mice that selectively lack ATG16L1 in keratinocytes ($\Delta^{Ker}atg16l1$ mice) [11] as ATG16L1-deficient mice die shortly after birth, precluding the study of ATG16L1 in adult murine tissues [12]. Mice lacking ATG16L1 in keratinocytes were highly sensitized to epidermal inflammation and inflammation-driven tumor formation. Moreover, $\Delta^{Ker}atg16l1$ mice exhibited precocious induction of hair growth, indicating altered HFSC activation kinetics. We show that prevention of autophagic responses in HFSCs not only expedites their activation, but also broadens their regenerative potential, enabling de novo HF formation in deep wounds and improving healing kinetics of more superficial wounds. Finally, we elucidated that heightened sensitivity of ATG16L1-deficient keratinocytes to apoptosis is the driving force of altered HFSC activation, thereby identifying regulated cell death as a central player in HF regeneration.

Results

Keratinocyte autophagy dampens skin inflammation

To investigate the role of autophagy in keratinocytes, mice with a "floxed" Atg16l1 gene were crossed to the Keratin-5 (KRT5) Cre line to generate keratinocyte-selective ATG16L1-deficient mice ($\Delta^{Ker}atg16l1$ mice) (Fig. S1A). Although $\Delta^{Ker}atg16l1$ mice show no overt skin phenotype [11], we observed a thickened stratum corneum relative to control mice (Fig. S1B, C), pointing to putative defects in desquamation which are in agreement with observations made in skin of mice lacking ATG7, another critical autophagy mediator, in keratinocytes [13]. Epidermal thickness, measured as the distance between the basement membrane and start of the stratum corneum, did not differ between $\Delta^{Ker}atg16l1$ mice and control littermates (Fig. S1D). The formation and maintenance of the epidermal permeability barrier was not compromised by lack of keratinocyte autophagy as assessed by transepidermal water loss measurements in neonatal and adult $\Delta^{Ker}atg16l1$ and control littermates (Fig. S1E-I).

As autophagy has been shown to mediate immune responses [14], we subjected $\Delta^{Ker}atg16l1$ and control mice to a topical inflammatory challenge by treating back skin of mice with the phorbol ester TPA (12-O-tetradecanoylphorbol-13-acetate) every other day for 11 days and monitored skin barrier perturbation over time (Figure 1A). TPA-treated

$\Delta^{Ker}atg16l1$ mice showed a markedly exacerbated inflammatory response as the skin of these mice displayed more erythema and scaling compared to control (Cre-negative $Atg16l1^{fl/fl}$) skin (Figure 1B). This exacerbated inflammatory response in $\Delta^{Ker}atg16l1$ skin was also apparent by the more pronounced thickening of the epidermis, higher transepidermal water loss and elevated levels of circulating IL6 (interleukin 6) (Figure 1C-F). To assess whether a partial reduction of ATG16L1 in keratinocytes is sufficient to alter the inflammatory skin response to TPA, we subjected heterozygous $\Delta^{Ker}Atg16l1^{fl/+}$ and Cre-negative $Atg16l1^{fl/+}$ control mice to repetitive topical TPA treatment and observed no differences in skin barrier perturbation nor epidermal thickness (Fig. S1J, K). Immunophenotyping by flow cytometric analyses revealed a marked increase of inflammatory macrophages (ITGAM/CD11b^{hi} ADGRE1/F4/80^{hi}) in TPA-treated $\Delta^{Ker}atg16l1$ skin compared to control skin, while the amount of other prominent immune cell populations did not differ between genotypes (Figure 1G, Fig. S2A). As polymorphisms in the human ATG16L1 gene have been linked to psoriasis [7], we assessed whether $\Delta^{Ker}atg16l1$ skin was also sensitized to psoriasiform inflammation, by subjecting mice to repetitive topical treatments with imiquimod, a TLR7 (toll-like receptor7) and TLR8 ligand, inducing psoriasis-like inflammation in mouse skin [15]. Upon imiquimod exposure, $\Delta^{Ker}atg16l1$ skin displayed a more pronounced perturbation of the epidermal barrier than control littermates as demonstrated by a more thickened epidermis and higher TEWL increase (Figure 1H,I), again indicating exacerbated inflammatory responses in skin of mice with autophagy-deficient keratinocytes.

Immunoblotting of primary mouse keratinocytes (PMKs) isolated from $\Delta^{Ker}atg16l1$ and control skin confirmed the absence of ATG16L1 protein and the impairment of autophagic signaling as shown by the absence of MAP1LC3/LC3 (microtubule-associated protein 1 light chain 3) processing in PMKs derived from $\Delta^{Ker}atg16l1$ mice (Figure 1J). To assess the cell-intrinsic responses of ATG16L1-deficient keratinocytes to inflammatory stimulation, we performed qPCR analysis on PMKs obtained from $\Delta^{Ker}atg16l1$ and control skin. TPA treatment of these cell cultures induced the expression of various cytokines and inflammatory mediators in both ATG16L1-proficient and -deficient PMKs. However, ATG16L1-deficient keratinocytes showed higher levels of Tnf and Cxcl10 compared to control keratinocytes (Fig. S2B), indicating a cell-intrinsic exacerbation of the inflammatory response in keratinocytes in absence of autophagy.

Together, these findings reveal the significance of the autophagy program specifically in keratinocytes in dampening inflammatory skin responses.

Enhanced tumor formation in mice lacking ATG16L1 in keratinocytes

Autophagy modulates cancer development and progression in a context- and tissue-dependent manner [16,17]. As we observed altered inflammatory responses to TPA in $\Delta^{Ker}atg16l1$ skin, we next investigated the role of autophagy in inflammation-driven skin tumorigenesis. For this, we subjected $\Delta^{Ker}atg16l1$ and $Atg16l1^{fl/fl}$ mice to chemically-
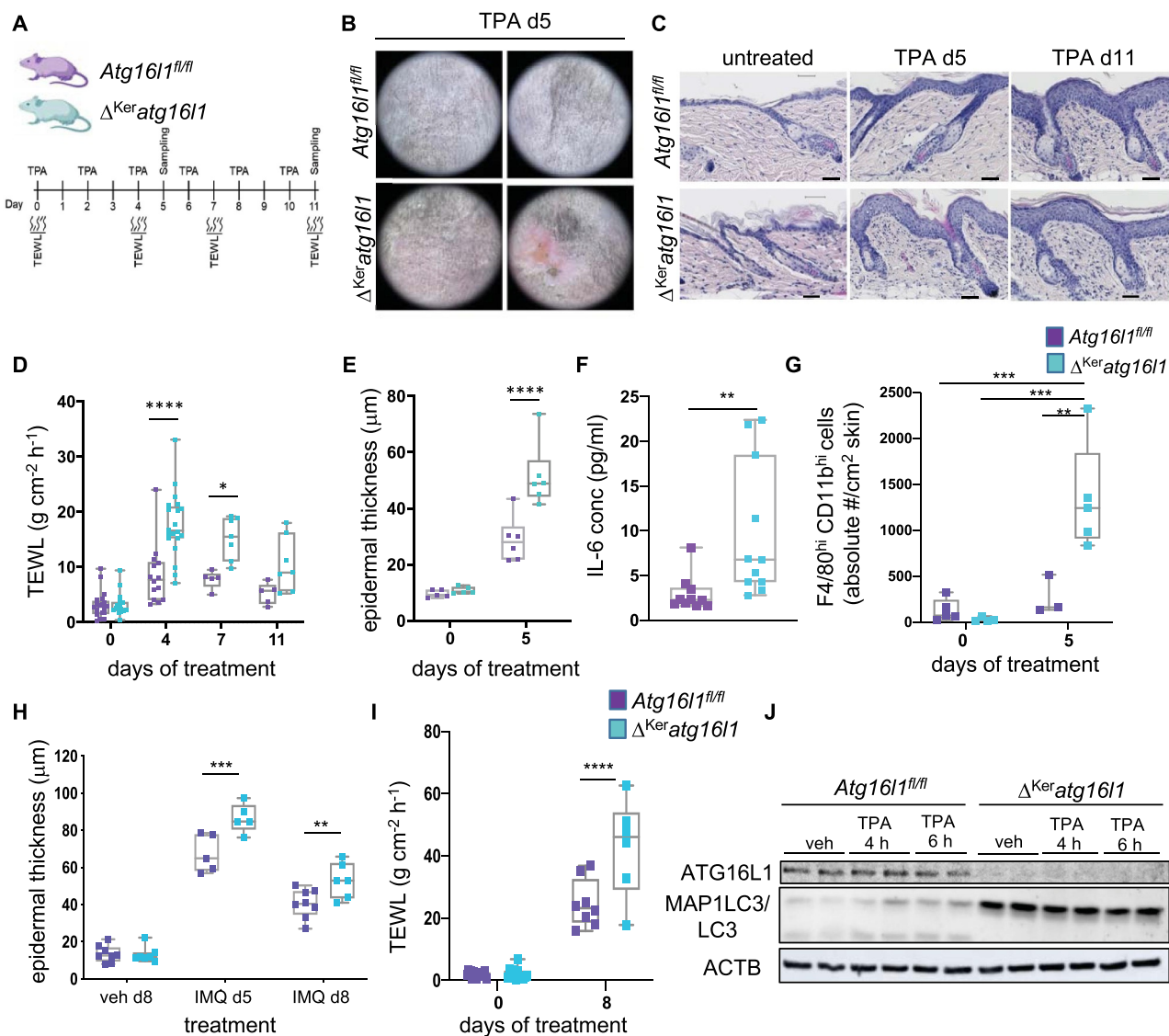
Figure 1. Exacerbated inflammatory responses in Δ^Ker^atg16l1 skin. (A) Schematic representation of the experimental set-up for inducing topical skin inflammation. (B) Representative dermatoscope images of back skin of control (Atg16l1^fl/fl^) and Δ^Ker^atg16l1 mice on day 5 of TPA treatment. (C) H&E-stained sections of untreated or TPA-treated skin of Atg16l1^fl/fl^ and Δ^Ker^atg16l1 mice. Scale bars: 100 μm. (D) Epidermal barrier function analysis by time-course measurements of transepidermal water loss (TEWL) (*p = 0.0104; ****p < 0.0001; two-way ANOVA with multiple comparisons; n ≥ 5 mice per condition). (E) Epidermal thickness measured on H&E-stained skin sections from untreated or TPA-treated Atg16l1^fl/fl^ and Δ^Ker^atg16l1 mice (n ≥ 5 mice per condition, for each biological replicate the mean of 10 measurements was taken; ****p < 0.0001; two-way ANOVA with multiple comparisons). (F) Levels of IL6 in serum of TPA-treated Atg16l1^fl/fl^ (n = 10) and Δ^Ker^atg16l1 (n = 12) mice at day 5 of the protocol (**p = 0.0011; Mann-Whitney testing). (G) Flow cytometric analysis of the absolute amount of F4/80^hi^ CD11b^hi^ immune cells per cm² skin in control Atg16l1^fl/fl^ and Δ^Ker^atg16l1 mice (n ≥ 3 mice per condition; ** p = 0.0016; ***p < 0.0001; two-way ANOVA with multiple comparisons). (H) Epidermal thickness measured on H&E-stained skin sections from untreated or imiquimod (IMQ)-treated Atg16l1^fl/fl^ and Δ^Ker^atg16l1 mice. Data represent means ± SEM (n ≥ 5 mice per condition, for each biological replicate the mean of 10 measurements was taken; **p = 0.01; ***p = 0.0007; two-way ANOVA with multiple comparisons). (I) Time-course TEWL measurements of untreated and IMQ-treated mice (****p < 0.0001; two-way ANOVA with multiple comparisons; n ≥ 5 mice per condition). Data are box whisker plots showing all values. (J) Western blot of PMK lysates obtained from Atg16l1^fl/fl^ and Δ^Ker^atg16l1 skin and treated with TPA or vehicle (veh) for the indicated time-points followed by immunoblotting for ATG16L1, MAP1LC3/LC3 and ACTIN as a loading control.

induced skin carcinogenesis. Mice were treated once with the carcinogen DMBA (2, 4-dimethoxybenzaldehyde) and subsequently three times per week for 15 weeks with the tumor-promoting agent TPA [18]. In agreement with the exacerbated inflammation observed upon TPA treatment, Δ^Ker^atg16l1 mice were sensitized to DMBA/TPA-induced skin tumorigenesis. Δ^Ker^atg16l1 mice developed tumors at an earlier timepoint than control littermates (Figure 2A) with half of Δ^Ker^atg16l1 mice developing at least one tumor by week 6 of the treatment protocol, in contrast to Atg16l1^fl/fl^ control mice in which this took significantly

longer. Δ^Ker^atg16l1 mice also developed significantly more tumors relative to controls (Figure 2B,C). Immunoblotting for SQSTM1/p62, a substrate for autophagic degradation, confirmed its accumulation in untreated and DMBA/TPA-treated skin tumor samples from Δ^Ker^atg16l1 mice relative to control mice (Figure 2D), indicating that autophagy is a naturally occurring process in normal and tumor skin, which is blocked by ablation of ATG16L1 in keratinocytes. These data indicate that keratinocyte autophagy dampens neoplastic responses in the skin.
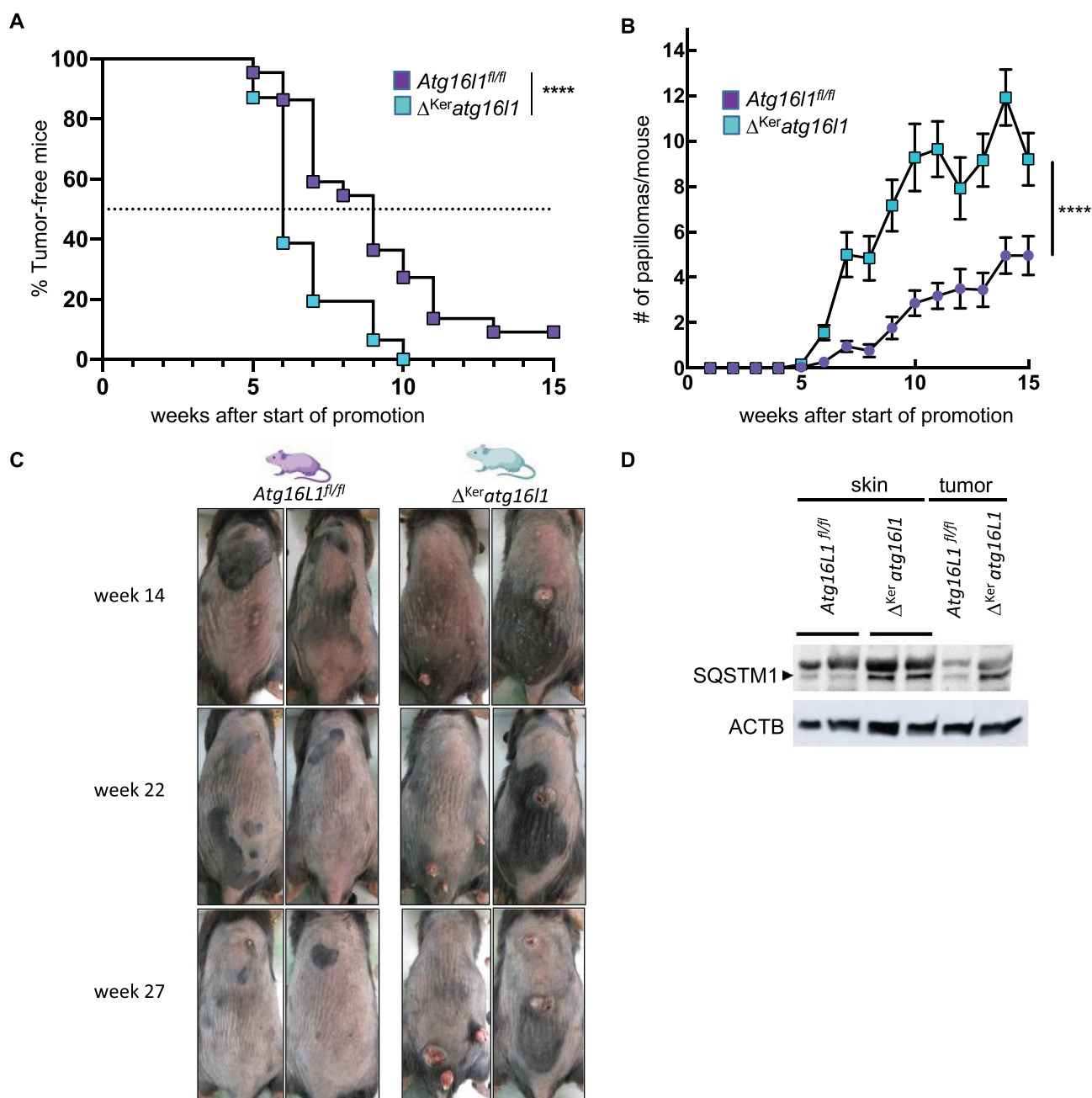
Figure 2. Keratinocyte autophagy protects skin from chemically-induced tumorigenesis. (A) Incidence of papilloma formation in *Atg16l1*^{fl/fl} (n= 22) and Δ[Ker]*atg16l1* (n= 25) mice treated with DMBA and TPA (Wilcoxon matched-pairs signed rank test; ****p< 0.0001). (B) Amount of papillomas per mouse in *Atg16l1*^{fl/fl} (n= 22) and Δ[Ker]*atg16l1* (n= 25) mice treated with DMBA and TPA (Wilcoxon matched-pairs signed rank test; ****p< 0.0001). Data represent means ± SEM. (C) Representative images of back skin of DMBA/TPA-treated *Atg16l1*^{fl/fl} and Δ[Ker]*atg16l1* mice at 14, 22 and 27 weeks after first TPA treatment. (D) Immunoblotting of SQSTM1/p62 in skin and tumor lysates of *Atg16l1*^{fl/fl} and Δ[Ker]*atg16l1* mice. Anti-ACTIN blot is shown as loading control.

Precocious onset of anagen in Δ[Ker]atg16l1 skin

To probe deeper into the cellular and molecular changes that occur in skin of Δ[Ker]*atg16l1* mice, we next performed single-cell RNA-sequencing (scRNAseq) of sorted live cells obtained from untreated total skin from 10-weeks-old control (Cre-negative *Atg16l1*^{fl/fl}) and Δ[Ker]*atg16l1* male littermates. Poor quality cells were removed based on pre-processing of the data according to the Marioni pipeline [19]. Unsupervised population clustering was performed as previously described [20] with high-affinity propagation based on expression of high variance genes (Figure 3A). Next, cell populations were annotated according to

the expression of cell-type markers as adapted from Joost *et al* [21]. (Fig. S3A, B). After determining which cells originated from Δ[Ker]*atg16l1* or control skin, a unique population of HF growth-associated keratinocytes was observed in Δ[Ker]*atg16l1* skin relative to age-matched littermate control skin (Figure 3B). Subclustering of the keratinocyte population and analysis of growth phase within these cells indeed revealed the unique presence of a proliferative HF population in Δ[Ker]*atg16l1* skin (Figure 3C-F). Differentially expressed gene (DEG) analysis of this cluster revealed upregulation of genes expressed by HF inner layer cells, more specifically germinative layer, medulla and cortex
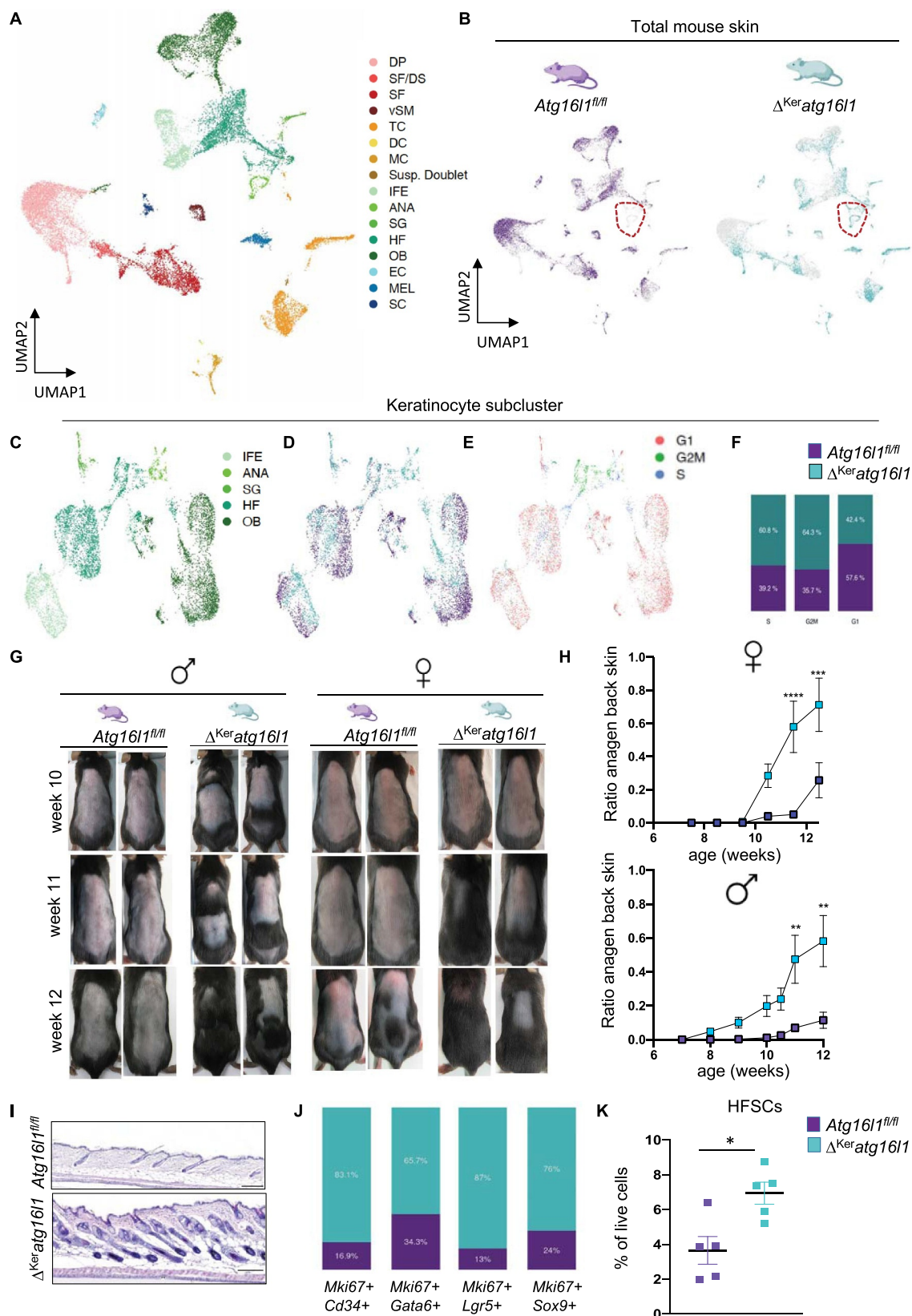
Figure 3. Altered HFSC activation kinetics in $\Delta^{Ker}atg16l1$ mice. (A) annotated UMAP clustering of scRNAseq data of live skin cells isolated from 10-weeks-old *Atg16l1*$^{fl/fl}$ and $\Delta^{Ker}atg16l1$ mice (DP: dermal papilla, DS: dermal sheet, SF: stromal fraction, vSM: vascular smooth muscle, TC: T-cells, DC: dendritic cell, MC: macrophage, Susp. Doublet: suspected doublet cells, LH: Langerhans cell, IFE: interfollicular epidermis, ANA: anagen, SG: sebaceous gland, HF: hair follicle, OL: outer layer, OB: outer bulge, EC: endothelial cell, LC: lymphatic cell, MEL: melanocyte, SC: Schwann cell). (B) Distribution of *Atg16l1*$^{fl/fl}$ and $\Delta^{Ker}atg16l1$ cells within the clusters. Dashed line delineates a keratinocyte population that is uniquely present in $\Delta^{Ker}atg16l1$ skin. (C) Annotated UMAP plot of keratinocyte subcluster from 10-weeks-old *Atg16l1*$^{fl/fl}$ and $\Delta^{Ker}atg16l1$ mice. (D) UMAP plot showing distribution of *Atg16l1*$^{fl/fl}$ and $\Delta^{Ker}atg16l1$ keratinocytes within this cluster. (E) UMAP plot indicating cell cycle stage of keratinocytes from both genotypes. (F) Bar plots showing relative percentage of *Atg16l1*-proficient or -deficient keratinocytes in different cell stages. (G) Representative photographs of the back skin of male and female *Atg16l1*$^{fl/fl}$ and $\Delta^{Ker}atg16l1$ littermates at week 10, 11 and 12 of age shaved at 7 weeks of age. (H) Ratio of the surface of anagen back skin to total shaved area in female and male *Atg16l1*$^{fl/fl}$ and $\Delta^{Ker}atg16l1$ mice ($n > 10$ per genotype; **$p < 0.01$; ***$p = 0.0002$;

keratinocytes, such as *Lef1, Mt2, Dcn, Id1, Krt27, Krt35* and others (Fig. S3C). At 10 weeks of age, mouse skin is in long telogen, the resting stage of the HF, and inner layer HF keratinocytes are not present at this stage [21]. Our scRNAseq data indicate that hair cycling is already molecularly induced at this time-point in Δ^{Ker}*atg16l1* skin, but not in control skin. We also observed notable changes in gene expression and cell composition between sebaceous gland (SG) keratinocytes from Δ^{Ker}*atg16l1* and control skin (Figure 3A,B), corroborating previous reports showing an important role for autophagy in sebum production and profile [22].

Monitoring of the hair cycle in Δ^{Ker}*atg16l1* and control littermates confirmed the precocious onset of anagen in Δ^{Ker}*atg16l1* mice in both males and females, indicating that keratinocyte autophagy critically contributes to the timing at which quiescent HFSCs are reactivated to initiate a new hair cycle (Figure 3G-I). This premature anagen onset was also apparent when we quantified the relative amount of proliferative (*Mki67*$^+$) HFSCs (*Cd34*$^+$, *Lgr5*$^+$, *Sox9*$^+$) observed in our scRNAseq data, which was markedly higher in Δ^{Ker}*atg16l1* skin compared to control skin (Figure 3J). Finally, flow cytometric analysis on epidermal cell suspensions of Δ^{Ker}*atg16l1* and control skin of 8 weeks-old mice revealed an increase in the number of HF stem and progenitor cells in skin of Δ^{Ker}*atg16l1* mice at a time-point when skin was phenotypically still in telogen (Figure 3K), while other keratinocyte SC populations did not differ between genotypes (Fig. S3D). The altered hair cycling kinetics were not due to the presence of the KRT5Cre transgene, since KRT5Cre transgenic mice carrying no floxed alleles showed normal hair cycling kinetics (Fig. S3E). Heterozygous expression of ATG16L1 in keratinocytes also did not result in changes in hair cycle kinetics (Fig. S3F).

Together, our analyses on Δ^{Ker}*atg16l1* skin identify keratinocyte autophagy as a crucial regulator of HFSC quiescence during telogen. When the autophagic flux is defective in keratinocytes, HFs undergo premature activation thereby accelerating anagen induction.

Keratinocyte autophagy controls production of HF growth mediators in the dermal papilla

Activation of HFSCs depends on reciprocal signaling between HFSCs and a specific population of fibroblasts that constitutes the dermal papilla (DP) [3]. To probe for putative fibroblast-derived factors mediating precocious anagen induction in Δ^{Ker}*atg16l1* skin, we subclustered and annotated the fibroblast population from our scRNAseq dataset and observed that the DP of Δ^{Ker}*atg16l1* and *Atg16l1*$^{fl/fl}$ mice separates into two distinct populations (Figure 4A,B). DEG analysis revealed that the top upregulated gene in DP fibroblasts from Δ^{Ker}*atg16l1* skin compared to wild-type DP fibroblasts is *Gas6* (Figure 4C). GAS6 (growth arrest specific 6) is a secreted factor regulating stress-induced HFSC activation

and growth [23]. Expression levels of other critical mediators of hair growth produced by the DP, such as *Scube3* [24], were also enhanced in DP fibroblasts from Δ^{Ker}*atg16l1* mice (Figure 4C). In agreement, markers that are typically expressed by telogen DP fibroblasts, such as *Pappa2* and *Crabp1* were upregulated in control fibroblasts compared to fibroblasts from Δ^{Ker}*atg16l1* mice (Figure 4D).

The preferred ligand of GAS6 is AXL, a member of the TYRO3, AXL and MERTK (TAM) family of receptor tyrosine kinases [25]. Inference of ligand-receptor interactions originating from DP fibroblasts and mediating transcriptional changes in keratinocytes, was performed by NicheNet analysis [26]. The top predicted ligand which we identified by the NicheNet algorithm to mediate DP-keratinocyte interactions, was GAS6 (Figure 4E), further validating the importance of this pathway in mediating hair growth. Indeed, known downstream targets of the GAS6-AXL signaling axis, such as *Ccnb1*, *Rad51* and *Cdk1*, are highly upregulated in ATG16L1-deficient anagen keratinocytes (Figure 4F).

In conclusion, scRNAseq analysis of total skin of Δ^{Ker}*atg16l1* and control littermates elucidated that the precocious induction of hair growth in Δ^{Ker}*atg16l1* skin is accompanied by upregulation of growth signals from the dermal papilla. These data identify keratinocyte autophagy as an important molecular program that dampens the production of HF growth signals by DP fibroblasts in telogen skin.

Autophagy curtails HFSC plasticity

In skin, two spatially and functionally distinct populations of keratinocyte SCs exist. The EpdSCs are located in the IFE and provide and maintain the epidermal permeability barrier, while the HFSCs reside in the HF and sustain growth and maintenance of the hair. Upon wounding of the skin, however, several of these HFSCs are mobilized to regions where they normally do not reside to exert functions that differ from their homeostatic roles, a phenomenon that is termed stem cell plasticity [4,27,28]. Recently, lineage tracing studies have revealed that deep wounds, such as full-thickness skin wounds, are largely re-epithelialized by EpdSCs, while shallow and intermediate wounds, are quicky infiltrated by HFSCs [29]. In Δ^{Ker}*atg16l1* mice, we observed precocious onset of anagen after full-thickness wounding, indicating that lack of ATG16L1 not only expedites HFSC activation in physiological conditions, but also in conditions of skin regeneration (Figure 5A). However, similar healing kinetics of full-thickness wounds were observed in Δ^{Ker}*atg16l1* and control mice (Figure 5B), conversely to what has been reported in mice lacking *Atg5* or *Atg7* selectively in keratinocytes [30]. Also, the restoration of the epidermal permeability barrier was similar over the healing course of full-thickness skin wounds in Δ^{Ker}*atg16l1* and control mice (Figure 5C). These full-thickness 8 mm punch biopsy wounds normally do not result in the formation of

---

****$p < 0.0001$; two-way ANOVA testing with multiple comparisons). **(I)** H&E-stained sections of 10-weeks old male *Atg16l1*$^{fl/fl}$ and Δ^{Ker}*atg16l1* back skin. Scale bars: 200 μm. **(J)** Relative percentages of proliferating (Ki67$^+$) SC populations in *Atg16l1*$^{fl/fl}$ and Δ^{Ker}*atg16l1* mice. **(K)** Flow cytometric analysis of HFSCs as percentage of live cells in 8-weeks-old *Atg16l1*$^{fl/fl}$ and Δ^{Ker}*atg16l1* mice (*n* = 5 mice per condition; *p = 0.0137; Mann-Whitney testing).
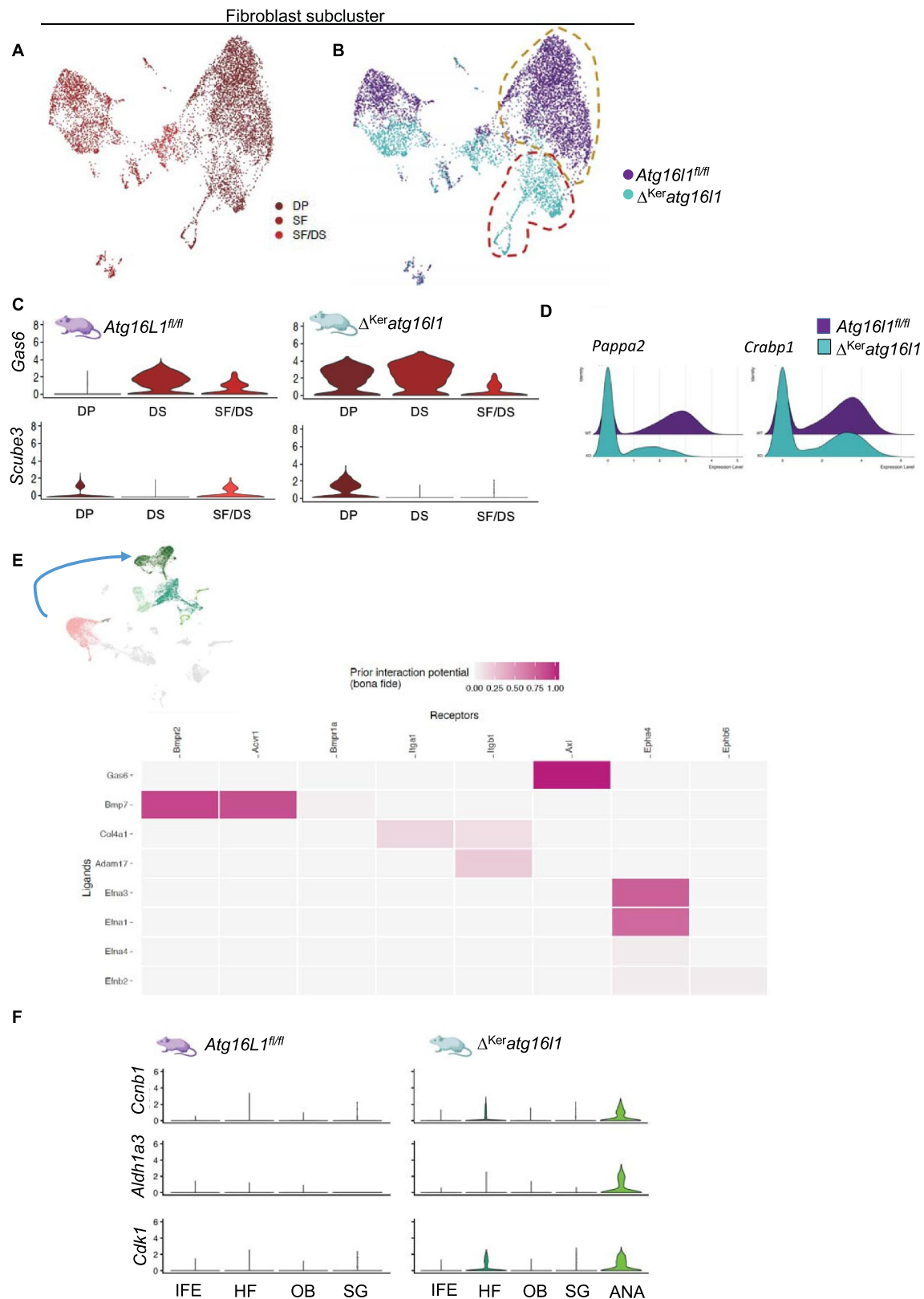
Figure 4. Keratinocyte autophagy dampens Gas6 expression levels in the telogen DP. (A) Annotated UMAP clustering of scRNAseq data of fibroblasts isolated from 10-weeks-old *Atg16l1^fl/fl* and Δ^Ker*atg16l1* mice (DP: dermal papilla, DS: dermal sheet, SF: stromal fraction). (B) Distribution of *Atg16l1^fl/fl* and Δ^Ker*atg16l1* fibroblasts within the clusters with indication of a unique DP population present in Δ^Ker*atg16l1* skin (dashed red line; dashed yellow line indicates the DP population in control skin). (C) Violin plots indicating the expression levels of the known HF growth factors *Gas6* and *Scube3* produced in different subsets of fibroblasts as determined by scRNAseq. (D) Ridgeline plot showing expression levels of *Pappa2* and *Crabp1* in fibroblasts of *Atg16l1^fl/fl* and Δ^Ker*atg16l1* mice. (E) Schematic representation of NicheNet analysis identifying ligands secreted by DP fibroblasts that bind on receptors expressed by keratinocytes, mediating gene expression changes. (F) Violin plots showing expression levels of the known GAS6-AXL target genes *Aldh1a3, Ccnb1* and *Cdk1* in different subsets of *Atg16l1^fl/fl* and Δ^Ker*atg16l1* keratinocytes as determined by scRNAseq.
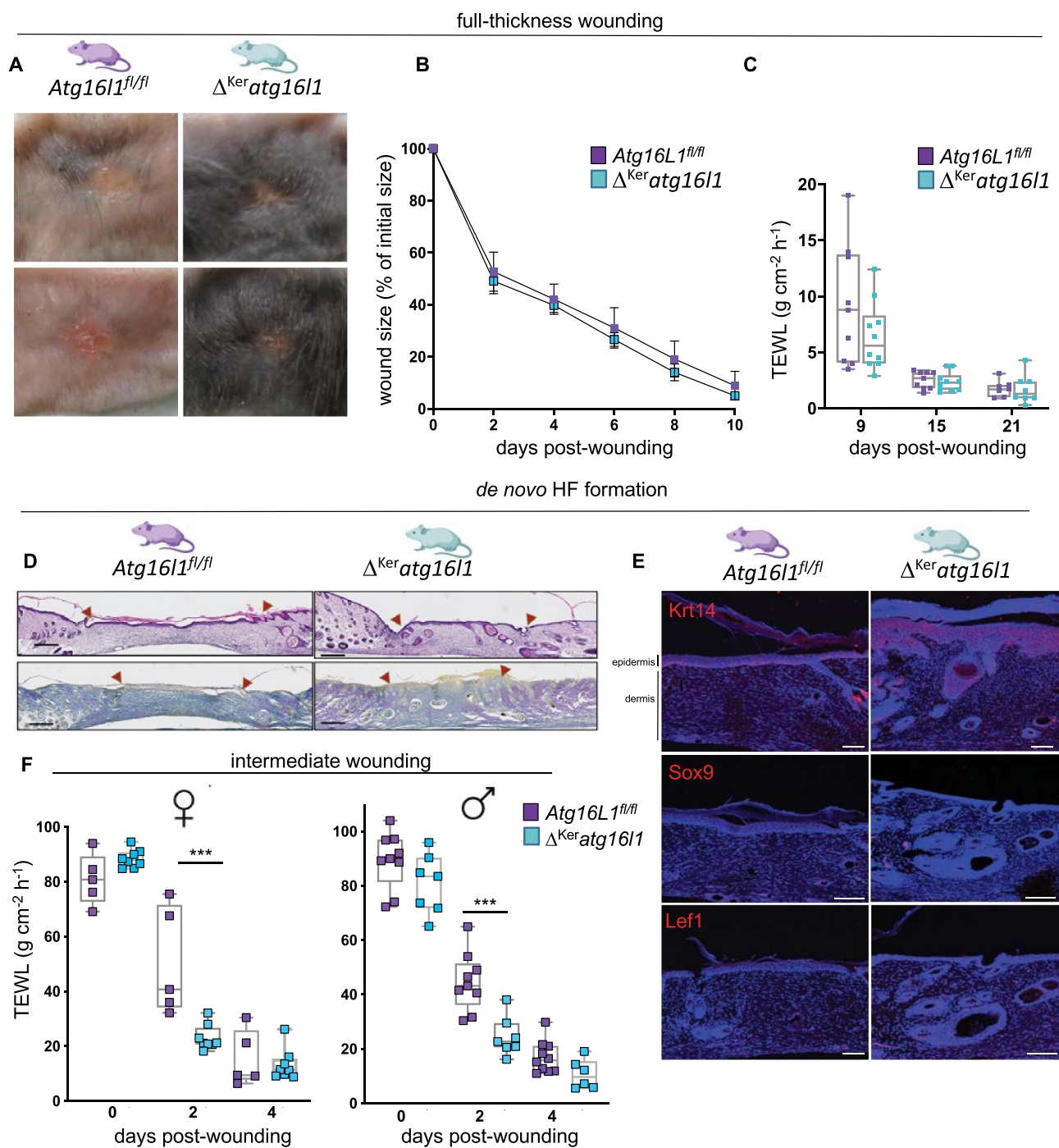
Figure 5. Altered regenerative responses in different subsets of keratinocyte SCs in $\Delta^{Ker}atg16l1$ mice. (A) Representative images of wound sites on the back skin of $Atg16l1^{fl/fl}$ and $\Delta^{Ker}atg16l1$ littermates at day 15 post-wounding. (B) Wound healing dynamics of $Atg16l1^{fl/fl}$ (n = 8) and $\Delta^{Ker}atg16l1$ (n = 9) mice after full-thickness skin wounding with an 8 mm punch biopsy (ns; two-way ANOVA with multiple comparisons). (C) Epidermal barrier function analysis by time-course measurements of transepidermal water loss (TEWL) on full-thickness wounds. (ns; two-way ANOVA with multiple comparisons; n ≥ 5 mice per condition). (D) H&E- (upper panels) and Herovici-stained (lower panels) skin sections of wounds of $\Delta^{Ker}atg16l1$ and control skin at day 15 post-wounding, showing *de novo* HF formation in $\Delta^{Ker}atg16l1$ remodeled skin. Scale bars: 200 μm. (E) Immunofluorescent staining for KRT14 , SOX9 and LEF1 on d15pw wounds of $Atg16L1^{fl/fl}$ and $\Delta^{Ker}atg16l1$ mice. Scale bars: 100 μm. (F) Epidermal barrier function analysis by time-course TEWL measurements on intermediate wounds in female and male $Atg16l1^{fl/fl}$ and $\Delta^{Ker}atg16l1$ mice (***p < 0.001; two-way ANOVA with multiple comparisons; n ≥ 5 mice per condition).

new HFs in the scar tissue of healing wounds [31,32]. Interestingly, *de novo* HF formation (often accompanied with cyst-like appearance) could be observed in the remodeling dermis of closed wounds of $\Delta^{Ker}atg16l1$ and not in control mice (Figure 5D,E), indicating that defective keratinocyte autophagy not only alters the activation kinetics of HFSCs but also broadens their functionalities. These newly

formed HF structures contain cells expressing SOX9, a typical HFSC and HF outer layer marker, and nuclear LEF1, the known effector of canonical Wnt signaling in HFSCs driving *de novo* HF formation [31].

As we observed altered activation kinetics of HFSCs in $\Delta^{Ker}atg16l1$ mice during hair cycling, we inflicted intermediate abrasive wounds on 7-weeks-old $\Delta^{Ker}atg16l1$ and control

skin to probe HFSC functionality in injury repair. Interestingly, we could observe improved skin barrier restoration in intermediate wounds inflicted on $\Delta^{Ker}atg16l1$ relative to control mice by time-course analysis of TEWL (Figure 5F).

Together, these data show that blocking autophagy in keratinocytes differentially affects the plasticity of EpdSCs and HFSCs in injury repair. While cutaneous repair responses of EpdSCs are similar in an autophagy-deficient versus proficient context, we show that HFSCs expand their regenerative potencies when their autophagic flux is blocked.

Heightened sensitivity to TNFRSF1A/TNFR1-mediated apoptosis in Δ^{Ker}atg16l1 skin underlies altered HFSC activation kinetics

ATG16L1-deficiency sensitizes macrophages and intestinal epithelial cells to cell death [12,33,34]. To investigate whether ATG16L1 can also protect keratinocytes from cell death, we stained skin sections of untreated and TPA-challenged $\Delta^{Ker}atg16l1$ and control mice for terminal deoxynucleotidyl transferase dUTP nick end labeling (TUNEL). We observed a higher number of TUNEL-positive cells in the interfollicular and in the follicular epidermis of both untreated and TPA-treated $\Delta^{Ker}atg16l1$ skin relative to the respective control skin (Figure 6A-C). Although enhanced cell death rates are present at baseline in $\Delta^{Ker}atg16l1$ skin, no epidermal erosion was observed as evidenced by normal epidermal thickness in these mice (Fig. S1D, Fig. S4A). During hair cycling, a significant population of keratinocytes located in the HF undergo coordinated cell death during catagen, the HF regression stage. Hence, we probed whether the sensitization of ATG16L1-deficient keratinocytes to apoptotic cell death was also present at this stage of non-immunogenic coordinated cell death. Quantification of cleaved CASP3 (caspase 3)-positive cells in catagen HFs in epidermal tail wholemounts obtained from $\Delta^{Ker}atg16l1$ and control littermates at P39 indeed revealed a significantly increased apoptotic cell death rate in skin of $\Delta^{Ker}atg16l1$ mice compared to control mice (Figure 6D).

Because increased epidermal cell death was observed in $\Delta^{Ker}atg16l1$ skin, we next addressed the cell-intrinsic pro-survival role of ATG16L1 using PMKs from $\Delta^{Ker}atg16l1$ and control skin. Western blotting on $\Delta^{Ker}atg16l1$ PMK lysates confirmed absence of ATG16L1, lack of LC3 processing and enhanced stability of SQSTM1, as is expected in conditions of compromised autophagy (Figure 6F). Already in basal conditions apoptotic cell death could be observed in $\Delta^{Ker}Atg16l1$ PMKs, but not in control PMKs, as shown by immunoblotting for cleaved CASP3. Moreover, $\Delta^{Ker}atg16l1$ PMKs were markedly sensitized to apoptotic cell death after stimulation with TNF (tumor necrosis factor). Pretreatment with the pan-caspase inhibitor zVAD-fmk induced necroptotic cell death to a similar extent in PMKs of both genotypes, as shown by immunoblotting for phospho-MLKL, which was inhibited by addition of the RIPK1 kinase inhibitor Nec1-s (Figure 6F). Stimulation of PMKs with the inflammatory agent TPA also

induced apoptosis in $\Delta^{Ker}atg16l1$ PMKs and not in control PMKs (Figure 6F), indicating that the increased sensitivity of ATG16L1-deficient keratinocytes to apoptotic cell death could be at the base of the exaggerated inflammatory responses induced by topical TPA treatment in $\Delta^{Ker}atg16l1$ mice.

Finally, to address whether the enhanced sensitization of ATG16L1-deficient keratinocytes to apoptotic death promoted the precocious activation of HFSCs observed in $\Delta^{Ker}atg16l1$ skin, we crossed the $\Delta^{Ker}atg16l1$ mice onto a CASP8 RIPK3-deficient ($casp8^{-/-}$ $ripk3^{-/-}$) genetic background in order to avoid embryonic lethality due to $Casp8$ deficiency [35,36]. The altered hair cycling kinetics that were observed in $\Delta^{Ker}atg16l1$ skin were indeed absent in compound $\Delta^{Ker}atg16l1$ $casp8^{-/-}$ $ripk3^{-/-}$ mice (Figure 6G), proving that the enhanced death of ATG16L1-deficient keratinocytes promotes the precocious activation of HFSCs. However, the thickening of the $stratum$ $corneum$ was still present in compound $\Delta^{Ker}atg16l1$ $casp8^{-/-}$ $ripk3^{-/-}$ mice (Fig. S4A), indicating that this phenotype of $\Delta^{Ker}atg16l1$ skin is not due to the cytoprotective role of keratinocyte autophagy. As TNFRSF1A/TNFR1-mediated cell signaling has been implicated in hair cycling [37], we tested whether compound depletion of TNFRSF1A/TNFR1 in $\Delta^{Ker}atg16l1$ mice obliterated early anagen onset. Monitoring of hair cycling indeed showed that the onset of anagen was normalized in $\Delta^{Ker}atg16l1$ $tnfrsf1a^{-/-}$ mice (Figure 6G). Together, our data identify the extent of TNF-induced apoptotic cell death as a key driver of anagen induction. Clearly, instructive signals originating from dying cells result in precocious DP activation and subsequent induction of hair growth.

Discussion

Autophagy is a crucial survival and recycling program, and defects in autophagy may impair host defense and induce inflammatory responses [10,38]. In agreement, we show that ATG16L1-deficiency in keratinocytes promotes epidermal inflammation upon treatment with a topical inflammatory agent. As the molecular mechanisms underlying inflammatory responses in the skin also partly mediate tumor formation [4], $\Delta^{Ker}atg16l1$ mice are also shown to be sensitized to inflammation-driven carcinogenesis induced by DMBA/TPA treatment, in agreement with previous studies in $\Delta^{Ker}atg7$ mice [39]. However, we observed a higher number of tumors per mouse in $\Delta^{Ker}atg16l1$ relative to control skin, which is opposite to what has been described in $\Delta^{Ker}atg7$ skin. This discrepancy may be explained by autophagy-independent functions of ATG16L1, such as intracellular trafficking [40], although this remains to be investigated.

The HF represents a highly relevant model structure to study adult SC biology, as this mini-organ harbors various well-defined SC populations that exhibit remarkable plasticity and regenerative capabilities [5,6]. SCs present in the basal layer of the interfollicular epidermis are highly active, as they provide for the continuous renewal of the epidermis and hence maintain the skin barrier. Conversely, SCs present in the HF are quiescent for most of the hair cycle and proliferate
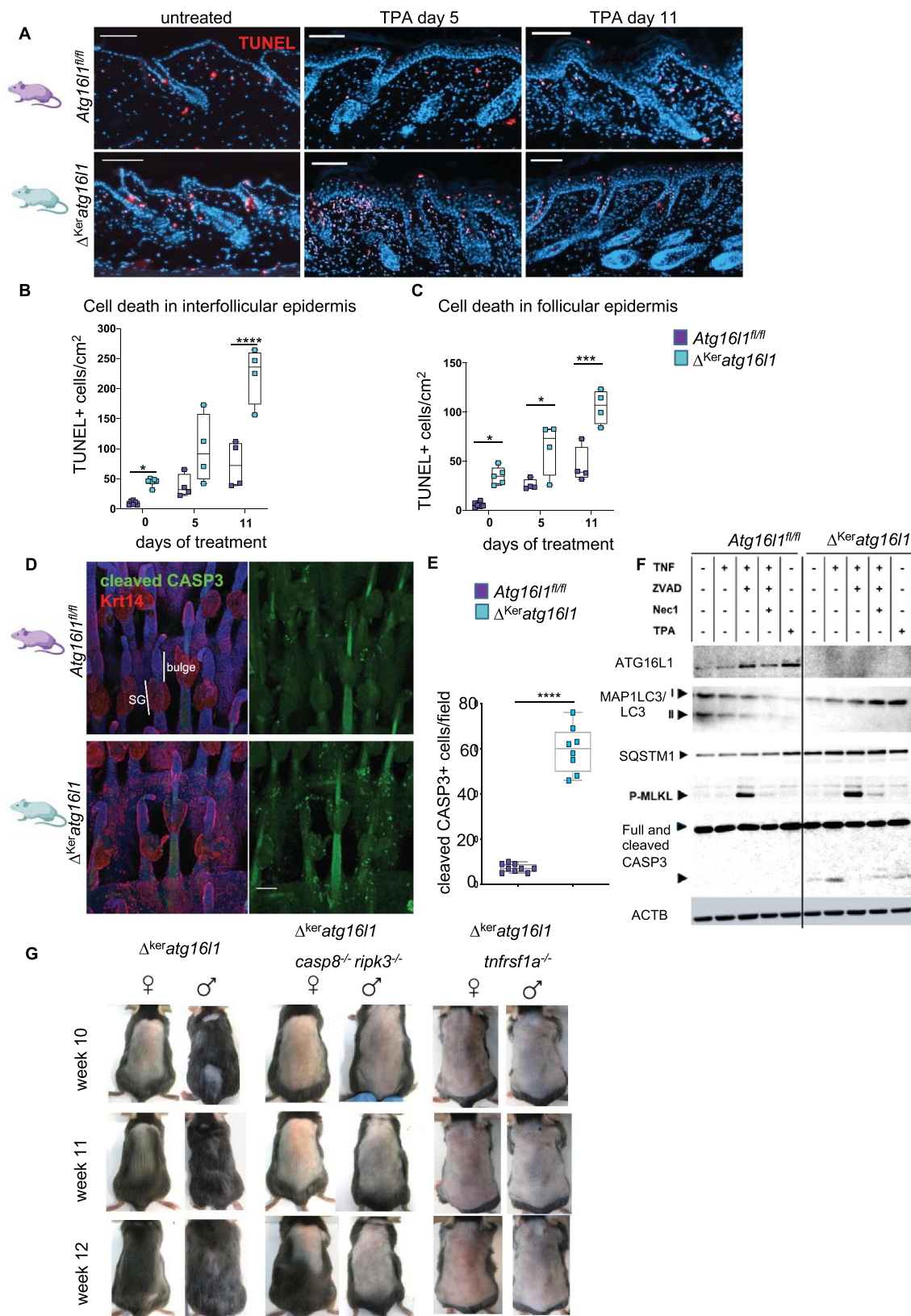
Figure 6. Enhanced sensitivity of ATG16L1-deficient keratinocytes to cell death underlies altered HFSC activation. (A) TUNEL-stained skin sections of *Atg16l1*^fl/fl^ and Δ^Ker^*atg16l1* untreated and TPA-treated mice. Scale bars: 200 μm. (B) Quantification of the number of TUNEL-positive interfollicular epidermis (IFE) cells in untreated and TPA-treated *Atg16l1*^fl/fl^ and Δ^Ker^*atg16l1* mice (*n* > 4 per genotype; * *p* = 0,0152; **** *p* < 0.0001; two-way ANOVA with multiple comparisons). (C) Quantification of the number of TUNEL-positive follicular epidermal cells in untreated and TPA-treated *Atg16l1*^fl/fl^ and Δ^Ker^*atg16l1* mice (*n* > 4 per genotype; **p* < 0.05; ****p* = 0.0002; two-way ANOVA with multiple comparisons). (D) Immunofluorescent staining for cleaved CASP3 (green) and KERATIN-14 (Krt14; red) of tail wholemounts of catagen HFs (P44) from *Atg16l1*^fl/fl^ and Δ^Ker^*atg16l1* mice. Right panels show cleaved CASP3 staining only. SG: sebaceous gland. Scale bars: 100 μm. (E) Quantification of cleaved CASP3 positive cells in catagen samples of *Atg16l1*^fl/fl^ and Δ^Ker^*atg16l1* tail epidermis (*n* = 9 mice per condition; *p* < 0.0001; Mann-Whitney test). (F) immunoblotting for ATG16L1, MAP1LC3/LC3, SQSTM1/p62, phosphorylated MLKL (p-MLKL), full-length and cleaved CASP3 on lysates from PMKs isolated from *Atg16l1*^fl/fl^ and Δ^Ker^*atg16L1* mice. Cells were untreated or treated with TNF, zVAD-fmk, Nec1S or TPA. ACTIN blot is shown as loading control. (G) Representative photographs of the back skin of Δ^Ker^*atg16l1*, Δ^Ker^*atg16l1 casp8*^−/−^ *ripk3*^−/−^ and Δ^Ker^*atg16l1 tnfrsf1a*^-/-^ mice at the indicated ages.

in bouts during the early stages of the HF growth phase, termed anagen [2,41]. Crucial growth signals originating from the DP, a specialized population of fibroblasts located underneath the HF germ, instruct these HFSCs to proliferate [42]. Identifying the molecular signals that control the activation and plasticity of these different keratinocyte SC populations is crucial to our understanding of the skin's regenerative and neoplastic responses.

Autophagy functions as an essential gatekeeper of adult SC quiescence in the hematopoietic lineage [43]. Since we observed exacerbated inflammatory and neoplastic responses in $\Delta^{Ker}atg16l1$ skin, we questioned whether disruption of the autophagic machinery affects SC activation and function in the skin. For this, we investigated $\Delta^{Ker}atg16l1$ skin in conditions of heightened proliferative need, namely in the active growth stage of the hair cycle and during wound healing. We show that $\Delta^{Ker}atg16l1$ skin exhibits precocious activation of HFSCs resulting in earlier induction of anagen, demonstrating an important role for autophagy in HFSC control. Our findings in $\Delta^{Ker}atg16l1$ skin are conflicting with a previous report showing that pharmacological activation of autophagy induces HF growth [44]. We speculate that the compounds used to induce autophagy in this report also affect other pathways beyond autophagy that could alter hair cycling, such as protein synthesis and cell proliferation. An alternative explanation is that skin-resident cells other than keratinocytes are affected by these agents, leading to indirect changes in activation kinetics of HFSCs. We established that the altered HFSC activation dynamics $\Delta^{Ker}atg16l1$ skin depend on TNF-dependent cell death responses, as preventing cell death by genetic deletion of *Casp-8* and *Ripk3* or by deletion of *Tnfrsf1a/Tnfr1* normalized hair cycling dynamics in $\Delta^{Ker}atg16l1$ mice.

Finally, we show that inhibition of keratinocyte autophagy does not alter the wound closure kinetics of full-thickness skin wounds, but promotes the healing of abrasive wounds. Lineage tracing studies revealed that full-thickness skin wounds are mainly repopulated by EpdSCs, while more superficial abrasive wounds, in which parts of the hair bulge remain intact, are largely re-epithelialized by HFSCs [29]. Our data contradict previously reported differences in wound healing kinetics of full-thickness skin wounds in mice lacking ATG5 or ATG7 selectively in keratinocytes [30]. This discrepancy could be explained by the smaller wounds inflicted in this study (4 mm versus 8 mm punch biopsy), or by the limited amount of mice these authors used to monitor the highly variable process of wound closure.

We identified cell death responses as crucial determinants of HFSCs activation and SC plasticity. Moreover, we demonstrated that TNF is a major driver of HFSC activation via keratinocyte apoptosis in ATG16L1-deficient conditions. Interestingly, ATG9A was recently identified as a crucial factor in detoxification of TNF and depletion of ATG9A from keratinocytes results in severe spontaneous skin inflammation, which is not observed in $\Delta^{Ker}atg16l1$ mice [11]. Cells dying by apoptosis can promote SC proliferation in tissues [45]. In skin, this link between cell death and SC activation seems counterintuitive, as HF regression -marked by extensive apoptosis [46]- is followed by a period of SC quiescence (telogen). During catagen, phagocytosis of apoptotic cells, also termed efferocytosis, occurs by neighboring keratinocytes [47]. It is therefore tempting to speculate that excessive cell death might result in insufficient clearance of dying cells in $\Delta^{Ker}atg16l1$ catagen skin, resulting in altered SC activation. In agreement, enhanced efferocytosis by dendritic cells in the skin was recently shown to promote injury repair [48]. Identifying the factors released by dying cells that mediate SC activation will be paramount for future therapeutic strategies aimed at exploiting this signaling axis for advancing cutaneous wound repair but also for putative treatment options for common hair loss diseases, such as alopecia areata and telogen effluvium.

Materials and methods

Mice

Atg16l1 floxed (*Atg16l1$^{fl/fl}$*) mice in which the third exon is flanked by LoxP sites were generated using EUCOMM embryonic stem cells (ES cell clone EPD0102_2_A02). $\Delta^{Ker}atg16l1$ mice were generated as previously described [11] by crossing *Atg16l1$^{fl/fl}$* mice to the KRT5Cre line [49]. Other mouse lines that were used are *casp8-deficient* mice [50], *tnfrsf1a/tnfr1-deficient* and *ripk3-deficient* mice [51]. All alleles were maintained on a C57BL/6J genetic background. Mice were housed in individually-ventilated cages at the VIB Center for Inflammation Research, in a specific pathogen-free animal facility. All experiments on mice were conducted according to institutional, national and European animal regulations. Animal protocols were approved by the ethical committee of the Center for Inflammation Research.

Wounding

Full-thickness skin wounds were inflicted on 7-weeks-old female and male mice after shaving of the back skin with an 8 mm punch biopsy. Wound sizes were measured with electronic callipers every other day by two independent researchers that were blinded to the genotypes. Intermediate wounds were inflicted on 7 to 8-weeks-old female mice by using a Dremel device as previously described [29]. Wounding procedures were repeated in three independent experiments with similar results and performed under analgesia and general anesthesia.

DMBA/TPA two-stage carcinogenesis

Chemical carcinogenesis experiments were performed as previously described [18]. Briefly, back skin of 7 to 8-week-old mice was shaved and treated once with 100 nmol DMBA (Sigma, D-3254) in 200 μl acetone. Seven days later, mice were treated with 6 nmol TPA (Sigma, P-8139) three times weekly for 15 weeks. Mice were allocated to groups based on genotypes, but housed in a randomized manner. Tumour incidence and burden were assessed once a week by two independent researchers who were blinded to the group allocations.

Topical application of imiquimod

Mice at 7 to 8 weeks of age were shaved and received a daily topical treatment on the back skin with 125 mg IMQ cream (Aldara^{TM}; 3 M Pharmaceuticals) or vehicle cream for 8 consecutive days.

Transepidermal water loss (TEWL) measurements

TEWL was measured on unwounded or wounded shaved back skin of adult anesthetised mice or on neonatal back skin using a TEWA meter (Courage and Khazaka, TM 210).

Primary keratinocyte isolation and culture

Primary mouse keratinocytes were isolated from $Atg16l1^{fl/fl}$ and $\Delta^{Ker}atg16l1$ skin as previously described [52]. Briefly, shaved adult back skin was isolated and subcutaneous fat was removed. Subsequently, skin was sterilized and floated on 0.25% trypsin overnight. Dermis was removed, epidermis was homogenized by vigorous pipetting and seeded on confluent feeder cultures. Cells were cultured in FAD medium (Bio&Sell): one part Ham's F12, three parts Dulbecco's modified Eagle's medium, 0.18 mM adenine, supplemented with 10% chelated fetal calf serum (Bodinco, S-FBS-EU-015) and a cocktail of 0.5 μg/ml hydrocortisone (Sigma, H4001), 5 μg/ml insulin (Sigma, I3536) and $1 \times 10-10$ M cholera enterotoxin (Sigma, C8052).

Histology

Skin tissue was dissected and fixed in 4% paraformaldehyde, dehydrated and embedded in paraffin. Sections were stained with hematoxylin/eosin (H&E) or with specific staining. Herovici staining was performed as previously described [53]. Following dewaxing, slides were incubated with Weigert's hematoxylin (Sigma, 1159730002) for 10 min to stain the nuclei. The sections were then stained for 3 min with Herovici staining solution (50 ml Van Gieson staining kit [Sigma, HT254], 50 ml Methyl blue [0.05% aq.; Sigma, M6900], 10 ml glycerol [Biosolve, 07122301] and 0.5 ml lithium carbonate [Sigma, 13010]). Slides were washed with 1% acetic acid for 2 min, followed by dehydration and mounting.

Immunofluorescence

Dewaxed paraffin sections were subjected to heat-mediated antigen retrieval (10 mM citrate buffer, pH 6). Skin sections or horizontal tail wholemounts were blocked with 2% BSA (Sigma, A2153), 0.02% fish gelatin (Sigma, G7765) and 10% rabbit serum (Sigma, R9133) for 1 h in PBS (Gibco, 14190–094) at room temperature. Sections were incubated with TUNEL reagent (Millipore, 17–141) according to the manufacturer's instructions, or with antibodies directed against cleaved CASP3 (Cell Signalling Technology, 9661), KRT14/keratin 14 (Santa Cruz Biotechnology, SC-53253), LEF1 (Cell Signalling Technology, 2230; C12A5) or SOX9 (Abcam, ab185230) overnight at 4°C in blocking solution, followed by 1 h incubation at room temperature with secondary antibodies (DyLight 555 goat-anti-rabbit, AlexaFluor 488 donkey-anti-mouse or combinations thereof; ThermoFisher, SA5–10033 and A-21202) and DAPI. Imaging was performed on an LSM880 confocal microscope (Zeiss).

Western blotting

Primary keratinocytes, skin or tumor tissue were homogenized using E1A lysis buffer (50 mM HEPES, pH 7.6, 250 mM NaCl, 5 mM EDTA, 0.5% NP40 [Sigma, 74385]) and NP40 buffer (50 mM Tris-HCl, pH 7.6, 1 mM EDTA, 150 mM NaCl, 1% NP40, 0.5% sodium deoxycholate [Sigma, D6750], 0.1% SDS) buffer respectively containing protease inhibitors (Roche, 11873580001) and phosphatase inhibitors (Roche, 04906837001), denatured in 1 × Laemmli buffer (50 mM Tris-HCl, pH 8.2; 2% SDS; 10% glycerol; 0.005% BPB; 5% β-mercaptoethanol) and boiled for 10 min at 95°C. Twenty μg of tissue lysates and 20 μg of cell lysates were separated by SDS-polyacrylamide gel electrophoresis (PAGE), transferred to nitrocellulose and analyzed by immunoblotting. Membranes were probed with antibodies against ATG16L1 (Cell Signalling Technology, 8089), SQSTM1/p62 (MBL, PM045), CASP3 (Cell Signalling Technology, 9662), ACTB/b-actin (Santa Cruz Biotechnology, sc -47,778).

Single-cell RNA sequencing and analyses

Single-cell suspensions were obtained from total skin as previously described [20]. Briefly, shaved back skin of mice was subjected to trypsin digestion for 1 hour at 37°C and subsequent digestion with collagenase type 1 (1.25 mg/ml, Invitrogen, 17100017), type 2 (0.5 mg/ml; Sigma, C2–22) and type 4 (0.5 mg/ml; Sigma, C5138) for 45 min. Live cells were sorted on FACS Aria, spun down and resuspended at a concentration of 1000 cells/μl. Cells at a target recovery of 10 000 cells were loaded on a GemCode Single-Cell Instrument (10× Genomics, Pleasanton). Single-Cell RNA-Seq libraries were generated by using GemCode Single-Cell 3'Gel Bead and Library kit (10× Genomics) according to the manufacturer's instructions. Sequencing libraries were loaded at 2.1 pM loading concentration on a NovaSeq6000 with custom sequencing metrics (single-indexed sequencing run, 28/8/0/91 cycles for R1/i7/i5/R2) (Illumina, San Diego, CA). Sequencing was performed at the VIB Nucleomics Core (VIB, Leuven, Belgium). Demultiplexing of the raw data and mapping to the mouse genome GRCm38.99 was done by the 10X CellRanger software (version 2.1.1; cellranger). Preprocessing of the data was done by the scran and scater R package according to workflow proposed by the Marioni and Theis lab [19]. Outlier cells identification was performed based on 3 metrics (library size, number of expressed genes and mitochondrial proportion). Cells were tagged as outliers when they were five median absolute deviations away from the median value of each metric across all cells, these low quality cells were removed from the analysis. Genes expressed in less than 3 cells and cells expressing less than 200 genes were removed. The samples were aggregated using the merge function,

counts were normalized and log2 transformed using the NormalizeData function, both from the Seurat R package (v3.1.0) using default parameters. Detecting highly variable genes, finding clusters and creating UMAP plots was done using the Seurat pipeline. Clustering was performed using the first 35 principal components and a resolution of 0.8.

Flow cytometry

Immunophenotyping of TPA-treated skin was performed on single-cell suspensions that were obtained as described above. Cells were stained with the following fluorochrome-linked antibodies: CD45-AF700, TCRγδ-AF488, L/D Amcyan, SIRPA-PerCP-Cy5, CD24-PacBlue, CD11b-BV605, XCR1-BV650, cD11c-BV711, F4/80-BV785, Ly6G-APC, MHCII-eFluor780, Siglec-F-PE, B220-BUV496, CD317-PE-Cy7, CD3-BUV395 and Fc receptor-blocking antibody CD16/CD32 (clone 2.4G2, BD Biosciences). Prior to measuring, counting beads (Life Technologies, C36950) were added to the cells. Measurements were performed on a BD Fortessa 5-laser cytometer and analyzed using FlowJo software (Tree Star). For quantifying different keratinocyte stem cell population in the skin, the epidermis was isolated from the back skin as previously described [52] and single-cell suspensions were stained with ITGA6/Itgα6-FITC (BD Biosciences, 555735), LY6A/Sca-1-PE (Ly-6A/E, BD Biosciences, 553108), CD34-eFluor 450 (eBiosciences, 48-0341-82) and eFluor780 as life/death marker.

Statistics

Results are expressed as box and whiskers plot indicating all datapoints or as means ± SEM. Statistical significance between *Atg16l1*^{fl/fl} and Δ^{Ker}*atg16l1* mice was assessed using Mann-Whitney testing, One-way ANOVA or Two-way ANOVA with multiple comparisons. Statistical analysis was performed with Prism software. For TEWL and epidermal thickness measurements, significance levels are only indicated between genotypes and not between time-points.

Data deposition

The accession number for the raw scRNA-sequencing data reported in this study is Gene Expression Omnibus (GeO): GSE218854.

Disclosure statement

No potential conflict of interest was reported by the author(s).

Funding

References

[1] Candi E, Schmidt R, Melino G. The cornified envelope: a model of cell death in the skin. Nat Rev Mol Cell Biol. 2005;6(4):328–340. doi: 10.1038/nrm1619

[2] Muller-Rover S, Foitzik K, Paus R, et al. A comprehensive guide for the accurate classification of murine hair follicles in distinct hair cycle stages. J Invest Dermatol. 2001;117(1):3–15. doi: 10.1046/j.0022-202x.2001.01377.x

[3] Greco V, Chen T, Rendl M, et al. A two-step mechanism for stem cell activation during hair regeneration. Cell Stem Cell. 2009;4 (2):155–169. doi: 10.1016/j.stem.2008.12.009

[4] Arwert EN, Hoste E, Watt FM. Epithelial stem cells, wound healing and cancer. Nat Rev Cancer. 2012;12(3):170–180. doi: 10.1038/nrc3217

[5] Donati G, Watt FM. Stem cell heterogeneity and plasticity in epithelia. Cell Stem Cell. 2015;16(5):465–476. doi: 10.1016/j. stem.2015.04.014

[6] Ge Y, Fuchs E. Stretching the limits: from homeostasis to stem cell plasticity in wound healing and cancer. Nat Rev Genet. 2018;19 (5):311–325. doi: 10.1038/nrg.2018.9

[7] Douroudis K, Kingo K, Traks T, et al. Polymorphisms in the ATG16L1 gene are associated with psoriasis vulgaris. Acta Derm Venereol. 2012;92(1):85–87. doi: 10.2340/00015555-1183

[8] Douroudis K, Kingo K, Traks T, et al. ATG16L1 gene polymorphisms are associated with palmoplantar pustulosis. Hum Immunol. 2011;72(7):613–615. doi: 10.1016/j. humimm.2011.03.009

[9] Gatica D, Lahiri V, Klionsky DJ. Cargo recognition and degradation by selective autophagy. Nat Cell Biol. 2018;20(3):233–242. doi: 10.1038/s41556-018-0037-z

[10] Deretic V. Autophagy in inflammation, infection, and immunometabolism. Immunity. 2021;54(3):437–453. doi: 10.1016/j.immuni.2021.01.018

[11] Huyghe J, Priem D, Van Hove L, et al. ATG9A prevents TNF cytotoxicity by an unconventional lysosomal targeting pathway. Science. 2022;378(6625):1201–1207. doi: 10.1126/science. add6967

[12] Saitoh T, Fujita N, Jang MH, et al. Loss of the autophagy protein Atg16L1 enhances endotoxin-induced IL-1β production. Nature. 2008;456(7219):264–268. doi: 10.1038/nature07383

[13] Rossiter H, König U, Barresi C, et al. Epidermal keratinocytes form a functional skin barrier in the absence of Atg7 dependent autophagy. J Dermatol Sci. 2013;71(1):67–75. doi: 10.1016/j. jdermsci.2013.04.015

[14] Cadwell K. Crosstalk between autophagy and inflammatory signalling pathways: balancing defence and homeostasis. Nat Rev Immunol. 2016;16(11):661–675. doi: 10.1038/nri.2016.100

[15] van der Fits L, Mourits S, Voerman JSA, et al. Imiquimod-induced psoriasis-like skin inflammation in mice is mediated via the IL-23/IL-17 axis. J Immunol. 2009;182(9):5836–5845. doi: 10.4049/jimmunol.0802999

[16] White E, Karp C, Strohecker AM, et al. Role of autophagy in suppression of inflammation and cancer. Curr Opin Cell Biol. 2010;22(2):212–217. doi: 10.1016/j.ceb.2009.12.008

[17] Poillet-Perez L, White E. Role of tumor and host autophagy in cancer metabolism. Genes Dev. 2019;33(11–12):610–619. doi: 10.1101/gad.325514.119

[18] Abel EL, Angel JM, Kiguchi K, et al. Multi-stage chemical carcinogenesis in mouse skin: fundamentals and applications. Nat Protoc. 2009;4(9):1350–1362. doi: 10.1038/nprot.2009.120

[19] Lun AT, McCarthy DJ, Marioni JC. A step-by-step workflow for low-level analysis of single-cell RNA-seq data with Bioconductor. F1000Res. 2016;5(2122):2122. doi: 10.12688/f1000research.9501.2

[20] Hoste E, Lecomte K, Annusver K, et al. OTULIN maintains skin homeostasis by controlling keratinocyte death and stem cell identity. Nat Commun. 2021;12(1):5913. doi: 10.1038/s41467-021-25944-2

[21] Joost S, Annusver K, Jacob T, et al. The molecular Anatomy of mouse skin during hair growth and Rest. Cell Stem Cell. 2020;26(3):441–457 e447. doi: 10.1016/j.stem.2020.01.012

[22] Rossiter H, Copic D, Direder M, et al. Autophagy protects murine preputial glands against premature aging, and controls their sebum phospholipid and pheromone profile. Autophagy. 2022;18(5):1005–1019. doi: 10.1080/15548627.2021.1966716

[23] Choi S, Zhang B, Ma S, et al. Corticosterone inhibits GAS6 to govern hair follicle stem-cell quiescence. Nature. 2021;592(7854):428–432. doi: 10.1038/s41586-021-03417-2

[24] Liu Y, Guerrero-Juarez CF, Xiao F, et al. Hedgehog signaling reprograms hair follicle niche fibroblasts to a hyper-activated state. Dev Cell. 2022;57(14):1758–1775.e7. doi: 10.1016/j.devcel.2022.06.005

[25] Wu Y, Singh S, Georgescu MM, et al. A role for Mer tyrosine kinase in $\alpha v \beta 5$ integrin-mediated phagocytosis of apoptotic cells. J Cell Sci. 2005;118(3):539–553. doi: 10.1242/jcs.01632

[26] Browaeys R, Saelens W, Saeys Y. NicheNet: modeling intercellular communication by linking ligands to target genes. Nat Methods. 2020;17(2):159–162. doi: 10.1038/s41592-019-0667-5

[27] Blanpain C, Fuchs E. Stem cell plasticity. Plasticity of epithelial stem cells in tissue regeneration. Science. 2014;344(6189):1242281. doi: 10.1126/science.1242281

[28] Sun X, Joost S, Kasper M. Plasticity of epithelial cells during skin wound healing. Cold Spring Harb Perspect Biol. 2022;15(5):a041232. doi: 10.1101/cshperspect.a041232

[29] Gonzales KAU, Polak L, Matos I, et al. Stem cells expand potency and alter tissue fitness by accumulating diverse epigenetic memories. Science. 2021;374(6571):eabh2444. doi: 10.1126/science.abh2444

[30] Qiang L, Yang S, Cui YH, et al. Keratinocyte autophagy enables the activation of keratinocytes and fibroblasts and facilitates wound healing. Autophagy. 2021;17(9):2128–2143. doi: 10.1080/15548627.2020.1816342

[31] Ito M, Yang Z, Andl T, et al. Wnt-dependent de novo hair follicle regeneration in adult mouse skin after wounding. Nature. 2007;447(7142):316–320. doi: 10.1038/nature05766

[32] Xue Y, Lim CH, Plikus MV, et al. Wound-induced hair Neogenesis model. J Invest Dermatol. 2022;142(10):2565–2569. doi: 10.1016/j.jid.2022.07.013

[33] Matsuzawa-Ishimoto Y, Shono Y, Gomez LE, et al. Autophagy protein ATG16L1 prevents necroptosis in the intestinal epithelium. J Exp Med. 2017;214(12):3687–3705. doi: 10.1084/jem.20170558

[34] Pott J, Kabat AM, Maloy KJ. Intestinal epithelial cell autophagy is Required to Protect against TNF-Induced apoptosis during Chronic Colitis in mice. Cell Host Microbe. 2018;23(2):191–202 e194. doi: 10.1016/j.chom.2017.12.017

[35] Oberst A, Dillon CP, Weinlich R, et al. Catalytic activity of the caspase-8–FLIPL complex inhibits RIPK3-dependent necrosis. Nature. 2011;471(7338):363–367. doi: 10.1038/nature09852

[36] Kaiser WJ, Upton JW, Long AB, et al. RIP3 mediates the embryonic lethality of caspase-8-deficient mice. Nature. 2011;471(7338):368–372. doi: 10.1038/nature09857

[37] Tong X, Coulombe PA. Keratin 17 modulates hair follicle cycling in a TN Fα-dependent fashion. Genes Dev. 2006;20(10):1353–1364. doi: 10.1101/gad.1387406

[38] Yamamoto H, Zhang S, Mizushima N. Autophagy genes in biology and disease. Nat Rev Genet. 2023;24(6):382–400. doi: 10.1038/s41576-022-00562-w

[39] Barresi C, Rossiter H, Buchberger M, et al. Inactivation of autophagy in keratinocytes Reduces tumor growth in mouse Models of epithelial skin cancer. Cells. 2022;11(22):3691. doi: 10.3390/cells11223691

[40] Ishibashi K, Uemura T, Waguri S, et al. Atg16L1, an essential factor for canonical autophagy, participates in hormone secretion from PC12 cells independently of autophagic activity. Mol Biol Cell. 2012;23(16):3193–3202. doi: 10.1091/mbc.E12-01-0010

[41] Hsu YC, Fuchs E. Building and Maintaining the skin. Cold Spring Harb Perspect Biol. 2022;14(7):a040840. doi: 10.1101/cshperspect.a040840

[42] Rompolas P, Mesa KR, Greco V. Spatial organization within a niche as a determinant of stem-cell fate. Nature. 2013;502(7472):513–518. doi: 10.1038/nature12602

[43] Ho TT, Warr MR, Adelman ER, et al. Autophagy maintains the metabolism and function of young and old stem cells. Nature. 2017;543(7644):205–210. doi: 10.1038/nature21388

[44] Chai M, Jiang M, Vergnes L, et al. Stimulation of hair growth by Small Molecules that Activate autophagy. Cell Reports. 2019;27(12):3413–3421 e3413. doi: 10.1016/j.celrep.2019.05.070

[45] Brock CK, Wallin ST, Ruiz OE, et al. Stem cell proliferation is induced by apoptotic bodies from dying cells during epithelial tissue maintenance. Nat Commun. 2019;10(1):1044. doi: 10.1038/s41467-019-09010-6

[46] Lindner G, Botchkarev VA, Botchkareva NV, et al. Analysis of apoptosis during hair follicle regression (catagen). Am J Pathol. 1997;151(6):1601–1617.

[47] Mesa KR, Rompolas P, Zito G, et al. Niche-induced cell death and epithelial phagocytosis regulate hair follicle stem cell pool. Nature. 2015;522(7554):94–97. doi: 10.1038/nature14306

[48] Maschalidi S, Mehrotra P, Keçeli BN, et al. Targeting SLC7A11 improves efferocytosis by dendritic cells and wound healing in diabetes. Nature. 2022;606(7915):776–784. doi: 10.1038/s41586-022-04754-6

[49] Tarutani M, Itami S, Okabe M, et al. Tissue-specific knockout of the mouse Pig-a gene reveals important roles for GPI-anchored proteins in skin development. Proc Natl Acad Sci U S A. 1997;94(14):7400–7405. doi: 10.1073/pnas.94.14.7400

[50] Salmena L, Lemmers B, Hakem A, et al. Essential role for caspase 8 in T-cell homeostasis and T-cell-mediated immunity. Genes Dev. 2003;17(7):883–895. doi: 10.1101/gad.1063703

[51] Newton K, Sun X, Dixit VM. Kinase RIP3 is Dispensable for normal NF-κBs, signaling by the B-Cell and T-Cell Receptors, tumor necrosis factor receptor 1, and Toll-like Receptors 2 and 4. Mol Cell Biol. 2004;24(4):1464–1469. doi: 10.1128/MCB.24.4.1464-1469.2004

[52] Jensen KB, Driskell RR, Watt FM. Assaying proliferation and differentiation capacity of stem cells using disaggregated adult mouse epidermis. Nat Protoc. 2010;5(5):898–911. doi: 10.1038/nprot.2010.39

[53] Herovici C. A polychrome stain for differentiating precollagen from collagen. Stain Technol. 1963;38:204–206.